Bioresource Technology 418 (2025) 131914

Contents lists available at ScienceDirect

Bioresource Technology

journal homepage: www.elsevier.com/locate/biortech

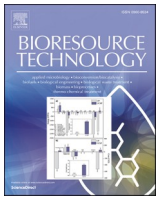

# Impregnation of granular activated carbon with nickel or copper improves performance of microbial electrosynthesis

Igor Vassilev [a], Hui Yao [a], Sadaf Shakeel [a], Markus Tuominen [a], Anne Heponiemi [b], Davide Bergna [b,c], Ulla Lassi [b,c], Marika Kokko [a,*]

[a] Faculty of Engineering and Natural Sciences, Tampere University, P.O. Box 541, FI-33104, Finland
[b] Research Unit of Sustainable Chemistry, P.O. Box 4300, FI-90014, University of Oulu, Finland
[c] University of Jyvaskyla, Kokkola University Consortium Chydenius, P.O. Box 567, 67701 Kokkola, Finland

## HIGHLIGHTS

- Microbial electrosynthesis (MES) for converting $CO_2$ to carboxylates was studied.
- Copper and nickel were used as catalysts on granular activated carbon (GAC).
- Metal impregnation of GAC improved $H_2$ evolution and its onset potential.
- Metal impregnation also improved drastically acetate production rates in MES.
- Changes in mass percentage of metal catalyst had a clear effect on MES performance.

## GRAPHICAL ABSTRACT

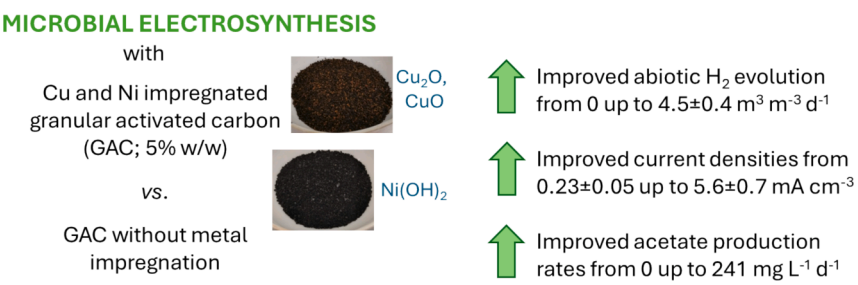


## ARTICLE INFO

*Keywords:*
Carboxylate production
Hydrogen evolution
Metal catalysts
Oxidation state

## ABSTRACT

Microbial electrosynthesis (MES) utilizes renewable electricity to power microbial conversion of carbon dioxide into multi-carbon products. As the cathode electrodes serve both as source of reducing equivalents and provide surface area for biofilm growth, the electrode material plays a crucial role in MES. In this study, granular activated carbon (GAC) was impregnated with copper or nickel (5 wt%) and used as MES cathode. In abiotic runs, metal impregnated GAC resulted in higher current densities, on average up to 5.6 mA $cm^{-3}$, compared to GAC without metal impregnation, up to 1.1 mA $cm^{-3}$. In MES, metal impregnated GAC enhanced acetate production rates compared to control GAC, up to 241 mg/L $d^{-1}$. The differences were mostly affected by the mass percentage of the metal catalyst on GAC, while the oxidation state of the metal had no considerable effect. Overall, impregnating GAC with metals shows high potential for improving the MES performance.

## 1. Introduction

A continuous rise in $CO_2$ emissions is a concern since it may lead to a rise in the sea level, ice sheets melting, and climate change. Annual global $CO_2$ concentration reached 416.7 ppm in 2021 and is on the course of further increase (Dadkhah and Tulliani, 2022). Microbial electrosynthesis (MES) appears as a promising solution for $CO_2$ mitigation. MES is a highly attractive bioelectrochemical application that converts $CO_2$ into value added carboxylates using microbes as biocatalysts at the cathode while providing reducing equivalents with an

* Corresponding author at: Faculty of Engineering and Natural Sciences, Tampere University, P.O. Box 541, FI-33104, Finland.
*E-mail address:* marika.kokko@tuni.fi (M. Kokko).

https://doi.org/10.1016/j.biortech.2024.131914
Received 5 September 2024; Received in revised form 27 October 2024; Accepted 28 November 2024
Available online 29 November 2024

external power source (Vassilev et al., 2018). Furthermore, MES provides a renewable way of producing short-chain fatty acids currently produced via fossil resources.

Performance of MES is highly dependent on the interaction between the electrocatalyst (*i.e.,* cathode) and the biocatalyst (*i.e.,* microorganism) and therefore, the choice of cathode material is crucial for achieving an efficient MES performance. Carbonaceous materials are highly used in MES as cathode due to their chemical stability, biocompatibility and cost-effective nature (Zhang et al., 2021). Among different carbon materials, granular activated carbon (GAC) is a promising choice because of its unique three-dimensional structure with low cost, high porosity, and high specific surface area and since it can provide number of sites to carry out electrocatalytic reactions (Caizán-Juanarena et al., 2019). These qualities make GACs an attractive cathode material which can support good interaction between electro- and biocatalyst and allows biofilm growth on its surface (Gibert et al., 2013; Kim et al., 2017). However, there are few limitations associated with GACs, such as low conductivity and mechanical instability (Zhang et al., 2021).

Transfer of electrons from cathode to microbial cells can take place either via direct or indirect pathways. In direct pathway, bacterial cells directly accept electrons from the cathode, while in indirect pathway a mediator (such as $H_2$) is formed at the cathode and acts as an electron carrier for the microbial cells. If the reducing equivalents are supplied via produced $H_2$ at the cathode, the $H_2$ evolution reaction can be enhanced by modification of the cathode, for example, via impregnation of catalytic metals, such as nickel (Ni) or copper (Cu) (Wang et al., 2019). Especially transition metals, such as iron, molybdenum, Ni and Cu, have been utilized to develop electroactive cathode electrodes (Vij et al., 2017). In MES, for example, nickel nanoparticles on a carbon cloth (Zhang et al., 2013) or nickel nanowire-coated graphite electrode (Nie et al., 2013) have improved the current density by 3.3- and 7.9-fold, respectively, and acetate production rate by 4.5- and 2.3-fold, respectively, as compared to the non-metallic electrodes. Nickel addition increased the conductivity and electron-exchange capacity of the Ni-modified graphite electrode simultaneously improving biofilm attachment (Nie et al., 2013). Furthermore, nickel-molybdenum alloys have been used as $H_2$-producing electrocatalysts to enhance acetate and methane production in MES (Kracke et al., 2019) and copper deposits on the surface of carbonaceous electrodes to enhance $H_2$ evolution in MES (Jourdin et al., 2016).

Such cathode modifications with metals have been mainly investigated using non-granular cathodes, while impregnation of GAC with metals may provide additional benefits, such as improving the conductivity of the GAC bed and charging the GAC bed homogeneously through the whole GAC bed promoting better MES performance, such as $H_2$ evolution, of the high-surface cathode (Chatzipanagiotou et al., 2022; Zhu et al., 2019). GAC has been decorated with iron oxides ($Fe_3O_4$), which improved the acetate production rate by 1.4-fold and current density by 1.5-fold due to the increased extracellular electron transfer and presence of electrochemically active bacteria (Zhu et al., 2019). The only study where nickel impregnated GAC were used in MES utilized nickel at high (5 %) and low (0.01 %) loading and reported a 25-fold increase in acetate production with the high Ni-loading compared to GAC without nickel (Chatzipanagiotou et al., 2022). While $Fe_3O_4$ and Ni impregnated GAC show promise in MES, the combination of other transition metals, such as Cu, with GAC has not been reported.

The oxidation states of the catalytic metals affect the mechanisms and efficiency of $H_2$ evolution reaction (HER). For example, when nanoscale nickel oxide/nickel (NiO/Ni) heterostructures were used for HER (Gong et al., 2014), it was suggested that NiO can serve as a good attachment site for $OH^-$ while Ni metal could facilitate $H^+$ adsorption, both of which steps are required for HER. CuO has also been utilized in chemical reactions where $H_2$ is either a product or a reactant, such as in water–gas shift reaction (Newsome, 1980) or methanol synthesis (Li et al., 1996). In MES utilizing Cu or Ni as catalysts, the oxidation state of the metal(s) used is rarely reported, although Chatzipangiotou et al. (Chatzipanagiotou et al., 2022) claimed that nickel oxide is formed in their experiment. However, revealing the oxidation state may help in understanding the mechanisms behind the (bio)electrocatalytic reactions.

This study examined the use of Ni and Cu as catalysts on GAC biocathodes in MES producing acetate from $CO_2$. The GAC with and without Cu and Ni impregnation (5 wt%, *i.e.,* mg $g^{-1}_{granule}$) were first characterized abiotically for the electrochemical and $H_2$ evolution performance. Next, the effect of Ni and Cu impregnation on the biological MES performance was determined in terms of volatility fatty acids (VFAs) production. The GAC with and without metal impregnation were fully characterized for total pore volume and pore size distribution before MES runs, and for the changes in specific surface area, Ni or Cu content, and oxidation states of the metals before and after the MES runs.

## 2. Materials and methods

### 2.1. Preparation of metal-impregnated electrode materials

Commercial Cyclecarb 305 (Chemviron) GAC was used as the bulk material for creation of metal modified GAC. GAC with a diameter of 0.63–1.00 mm was used to obtain sufficient conductivity, provide adequate space for biomass growth and to avoid clogging and accumulation of pressure. Three types of granules were used in the experiments: Cu modified granules (Cu-GAC), Ni modified granules (Ni-GAC), and unmodified granules (GAC). The metal impregnations of the commercial granules were performed through dry impregnation. Prior the dry impregnation of Cu and Ni, pore volumes (PVs) of commercial granules were measured as described in Section 2.2. The amount of metal salts, *i.e.,* $Cu(NO_3)_2{\cdot}(H_2O)$ (technical grade, assay $\geq$ 97 %) and $Ni(NO_3)_2{\cdot}6(H_2O)$ (technical grade assay $\geq$ 99 %) (VWR International BVBA, Geldenaaksebaan, Leuven, Belgium) were calculated so that the theoretical 5 % mass of metal to mass of GAC ratio was achieved. Cu and Ni nitrate salts were dissolved in an exact amount of water to fill the pore volume (PV) of commercial granules. Mixtures of metal salts and granules were impregnated for 5 h and after that, the produced mixture was placed in a ventilated oven and dried at 105 °C overnight. The dried material was then collected and placed in a stainless-steel reactor inserted in a tubular furnace Nabertherm RT 50/250/13-P320 (Lilienthal, Germany) for calcination at 500°C with a heating gradient of 4°C $min^{-1}$ and holding time of 2 h. During all the calcination process, the sample was under $N_2$ gas atmosphere. After the calcination, the reactor was cooled down overnight in inert atmosphere and then the carbon impregnated samples collected and stored under vacuum to avoid the oxidation of the metallic Cu and Ni nanoparticles.

### 2.2. Characterisation of electrode materials

Specific surface area (SSA), total PV and pore size distribution (PSD) were determined from nitrogen adsorption–desorption isotherms. Micromeritics 3Flex (Norcross, USA) instrument using $N_2$ gas as adsorbate was utilized for the physisorption. Before determining the isotherms, samples were degassed at 2 mmHg pressure and 140 °C for 3 h to remove previously adsorbed gases from the pores and to clean the sample surfaces. The isotherms were determined by placing degassed tubes into liquid nitrogen for achieving isothermal and cryogenic conditions and then adding small doses of nitrogen at the equilibrium. SSA was calculated by Brunauer-Emmet-Teller method (BET) (Brunauer et al., 1938) while total pore size and pore size distribution by non-local density functional theory (NLDFT) with a model specifically designed for carbon materials assuming slit geometry of the pores (Lastoskie et al., 1993).

The Cu and Ni content of the GAC was determined by using inductively coupled plasma optical emission spectroscopy (ICP-OES, Agilent 5110 SVDV, Agilent Technologies Inc, Santa Clara, California USA). Before analysis around 0.3 g of each sample was digested with 9 and 3

mL of concentrated $HNO_3$ and HCl, respectively at 180 °C for 10 min by using microwave oven (Milestone ETHOS UP, Milestone Srl, Sorisole (BG), Italy).

X-ray photoelectron spectroscopy (XPS) analysis was performed to observe the possible change in the oxidation states of the active metals by using Thermo Fisher Scientific ESCALAB 250Xi XPS System (Thermo Fisher Scientific,168 Third Avenue, Waltham, MA USA 02451) with the monochromatic AlKα radiation (1486.7 eV) operated at 20 mA and 15 kV. In the procedure, sample powders were placed on a gold sample holder and pass energy of 20 eV and spot size 900 μm were used to measure the Cu, Ni, O, C and Au for all samples. Avantage V5 software was used for the spectral analysis and C1s line at 248.8 eV was used as a calibration peak for the charge compensation.

### 2.3. Set-up and operation of microbial electrosynthesis

During abiotic experiments, the following medium was used: 18 g/L $Na_2HPO_4{\cdot}2H_2O$, 3 g/L $KH_2PO_4$, 3 g/L $NH_4Cl$, 15 mg/L $CaCl_2$, 20 mg/L $MgSO_4{\cdot}7H_2O$, 10 mL $L^{-1}$ trace element solution (1.5 g/L $C_6H_9NO_6$, 3 g/L $MgSO_4{\cdot}7H_2O$, 0.5 g/L $MnSO_4{\cdot}H_2O$, 1 g/L NaCl, 0.1 g/L $FeSO_4{\cdot}7H_2O$, 0.18 g/L $CoSO_4{\cdot}7H_2O$, 0.1 g/L $CaCl_2{\cdot}2H_2O$, 0.18 g/L $ZnSO_4{\cdot}7H_2O$, 10 mg/L $CuSO_4{\cdot}5H_2O$, 20 mg/L $KAl(SO_4)_2{\cdot}12H_2O$, 10 mg/L $H_3BO_3$, 10 mg/L $Na_2MoO_4{\cdot}2H_2O$, 30 mg/L $NiCl_2{\cdot}6H_2O$, 0.3 mg/L $Na_2SeO_3{\cdot}5H_2O$, 0.4 mg/L $Na_2WO_4{\cdot}2H_2O$, distilled $H_2O$ up to 1000 mL) and 1 mL $L^{-1}$ vitamin solution (2 mg/L biotin, 2 mg/L folic acid, 10 mg/Lpyridoxine-HCl, 5 mg/L thiamine-HCl, 5 mg/L riboflavin, 5 mg/L nicotinic acid, 5 mg/L D-Ca-pantothenate, 0.1 mg/L vitamin $B_{12}$, 5 mg/Lp-aminobenzoic acid, 5 mg/L lipoic acid, distilled $H_2O$ up to 1000 mL). For biological experiments, the aforementioned medium was amended with 2.1 g/L sodium 2-bromoethanesulfonate and 1 g/L yeast extract. 2-Bromoethanesulfonate is known to be efficient in locking the last step of methanogenesis by inhibiting methyl-CoM reductase reaction (Park et al., 2019). To remove surplus oxygen, both abiotic and biological media were sparged with $N_2$ for approximately 60 min/L before addition to the reactor.

The MES reactor was a ca. 250 mL elongated glass vessel consisting of three small outlets, one at the bottom and two at the side, and one big opening on top (see supplementary material) with a working volume of ca. 210 mL. The top opening was sealed tightly with a large rubber cap which was penetrated by a glass vial that acted as the anode chamber. The anode chamber was insulated from the rest of the reactor (*i.e.*, cathode chamber) by a cation exchange membrane (1.5 cm diameter, Membranes International, USA) placed at the bottom of the vial. Platinum wire (ca. 15 cm length, 0.40 mm diameter, 99.95 % purity, Advent research materials, UK) was used as the counter electrode and 50 mM $H_2SO_4$ as anolyte to decrease potential limitations related to the anode.

The cathode compartment consisted of ca. 32.5 mL GAC and a titanium mesh (ca. 4.7 cm diameter, 18 mesh woven from 0.28 mm diameter wire, Alfa Aesar, Germany) with titanium wire connection (length 11 cm, diameter 0.5 mm, 99.6+% purity, Goodfellow, Germany) was embedded in the middle of the GAC bed to act as a current collector. The granules were manually packed tightly between the titanium mesh and a plastic mesh ring structure (see supplementary material), which was supported from above by vertical plastic panels. The titanium mesh was supported from below by stationary glass beads that were held tightly in place by a plastic net. A RE-5B Ag/AgCl reference electrode (+0.206 V *vs.* normal hydrogen electrode, BASi, USA) was inserted to the GAC bed through a glass capillary filled with 3 M NaCl. The potentials are later on reported against Ag/AgCl reference electrode. The cathode potential was controlled at −0.85 V (except for the second run with Ni-GAC, where cathode potential was controlled at −0.85 V for the first three days, after which it was decreased to −0.755 V due to challenges in maintaining the potential) with a potentiostat (Bank Elektronik, Intelligent Controls GmbH, Germany). The reactors were run at 35 °C in duplicate that were operated in consecutive runs, *i.e.,* first and second run, both of which used fresh electrode materials.

The reactors were filled with 550 mL of $N_2$-sparged medium and 30 mL (ca. 5 %) of enrichment culture that had been grown in the laboratory for ca. four years, fed with $CO_2$ and was dominated by *Eubacterium* sp. (Vassilev et al., 2024). The cathodic medium was circulated through a recirculation bottle at a flow rate of 200 mL $min^{-1}$ (Masterflex L/S Digital Drive pump). The anode chamber was regularly supplied with fresh 50 mM $H_2SO_4$, while the glass capillary of the reference electrode was regularly supplied with fresh 3 M NaCl. $CO_2$ was introduced to the reactor by sparging the medium in the recirculation bottle with $CO_2$ in the beginning of the run and after that five days a week with a flow rate of 0.4 L $min^{-1}$ for 15 min.

The abiotic cathodes were characterized with cyclic voltammetry (CV) with a potentiostat (VMP3, BioLogic, France) at a scan rate of 0.01 mV/s within a potential window from −0.6 V to −0.87 V (Cu-GAC and Ni-GAC) or to −1.05 V (GAC) before each MES run. $H_2$ evolution was determined between the first CV and MES runs (without $CO_2$ feeding) by maintaining the cathode potential at −0.85 V for 21 h with VMP3 potentiostat and measuring the volume of $H_2$ produced. The $H_2$ evolution was measured in three consecutive runs with the same electrode materials, and the $H_2$ production rates were calculated against the reactor volume. To study how the force used to pack the GAC bed affects the contact resistance of the granules, a packed GAC bed (diameter of 0.63–1.00 mm, no metal impregnation) was pressed with different forces from 0.1 to 1.6 Nm and the contact resistance was determined.

### 2.4. Analyses and calculations

The catholyte pH was measured with WTW-330i pH meter (Germany) and optical density at 600 nm ($OD_{600nm}$) with UV–Vis spectrophotometer (UV-1800, Shimadzu, Japan). Volatile fatty acids (VFAs) were analyzed, after filtration through a 0.2 μm pore filter (CHROMAFIL Xtra PET, MACHERREY-NAGEL, Germany), with a gas chromatograph equipped with a flame ionization detector (GC-FID 2010 Plus, Shimadzu, Japan) and a Zebron ZB-WAX plus column (0.25 um diameter, 30 m length). Helium was used as a carrier gas with a flow rate of 84.4 mL $min^{-1}$. The injector and detector temperatures were 250 °C, and the column temperature was first kept at 40 °C for 2 min, increased to 160 °C min at a rate of 20 °C $min^{-1}$, and further increased to 220 °C with a rate of 40 °C $min^{-1}$. The gas content was measured with GC equipped with a thermal conductivity detector (GC-TCD 2014, Shimadzu, Japan) and Agilent J&W packed GC column (2.00 mm internal diameter, 1.8 m length). Nitrogen was used as carrier gas with a flow rate of 20 mL $min^{-1}$ and the injector, column, and detector temperatures were kept at 110 °C, 80 °C, and 110 °C, respectively. The gas volume in the gas bags was determined with a water displacement method.

The current densities were calculated against the apparent volume of the GAC used as cathode electrode, *i.e.*, 32.5 $cm^3$. $H_2$ onset potential was determined by drawing a tangent on the linear region of the CV curve and evaluating the cathode potential at 0 mA $cm^{-3}$. The cathodic efficiencies for acetate production were calculated as described by Yao et al. (2024).

## 3. Results and discussion

### 3.1. Abiotic characterization of metal-impregnated granules

The physisorption analysis showed a reduction in SSA and pore volume for the impregnated GAC mainly due to the intrusion of the active metal in the GAC structure (Table 1). Materials showed microporous structure and the difference in the pore size distribution between the samples was negligible indicating that the metals did not change the porous morphology of the GAC. While the intended Cu and Ni content was 5 wt%, the results show that the GAC contained 4.7 wt% Cu and 4.5 wt% Ni (Table 1).

The CVs of the original GAC were compared to the Cu and Ni impregnated GAC (Fig. 1). Without metal impregnation, current density of 0.8 mA $cm^{-3}$ was obtained at cathode potential of −0.88 V with a $H_2$

**Table 1**
Characteristics of the fresh Granular activated carbon (GAC) materials with and without metal impregnation, including specific surface area (SSA), pore volume, pore size distribution (PDS) and Cu and Ni content. GAC were impregnated with 5 wt% Cu (Cu-GAC) or Ni (Ni-GAC).

| | GAC | Cu-GAC | Ni-GAC |
|---|---|---|---|
| SSA ($m^2/g$) | 723 | 685 | 632 |
| Pore volume ($cm^3\ g^{-1}$) | 0.40 | 0.39 | 0.37 |
| Pore size (nm) | 2.33 | 2.35 | 2.43 |
| **PSD** | | | |
| Micropores, < 2 nm (%) | 65.8 | 64.6 | 63.9 |
| Mesopores, 2–50 nm (%) | 33.3 | 34.4 | 35.2 |
| Macropores, > 50 nm (%) | 0.87 | 1.01 | 0.83 |
| **Metal content** | | | |
| Cu (mg $g^{-1}_{granule}$) | 0.13 | 47.0 | 0.17 |
| Ni (mg $g^{-1}_{granule}$) | 0.05 | 0.08 | 45.0 |

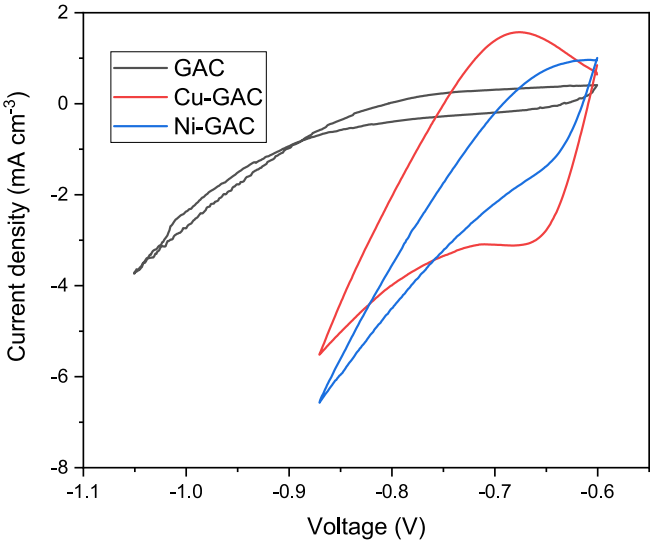


**Fig. 1.** Abiotic CVs of GAC impregnated with Cu (Cu-GAC) or Ni (Ni-GAC) and without (GAC) metal impregnation. CVs were run with a scan rate of 0.01 mV/s. The current densities are given against the volume of the GAC.

onset potential of ca. −0.80 V. Impregnating the GAC with Cu and Ni enhanced the current densities up to 5.5 and 6.6 mA $cm^{-3}$ at −0.88 V, respectively. Furthermore, the $H_2$ onset potentials were decreased to −0.75 and −0.69 V with Cu-GAC and Ni-GAC, respectively. Activated carbon has been widely studied due to its capacitive behavior that can arise either from charge separation at the electrical double-layer, *i.e.*, the electrode/electrolyte interface, or from pseudo-capacitance, *i.e.*, charge storage occurring due to reversible Faradaic reactions (Huang et al., 2007). For example, nickel-impregnated activated carbon (AC) cathodes were studied earlier for $H_2$ evolution in microbial electrolysis cells indicating pseudo-capacitive behavior of the Ni/AC particles, which was highest with the lowest nickel content (Moreno-Jimenez et al., 2023). It has been also reported earlier that introducing small amounts of nickel (hydroxide) to AC enhanced the specific capacitance of the electrode (Huang et al., 2007). The capacitive behavior of the metal impregnated GAC was also higher in this study compared to original GAC (Fig. 1).

To further study the $H_2$ evolution potential of the different GAC, $H_2$ production was studied for 21 h by fixing the cathode potential at −0.85 V (Fig. 2). $H_2$ mediated VFA production has been reported in various studies utilizing metal catalysts on MES cathodes (*e.g.*, de Smit et al., 2024; Jourdin et al., 2016; Kracke et al., 2019) and thus, a cathode potential enabling $H_2$ evolution with metal impregnated GAC was chosen for MES operation also in this study. As the abiotic $H_2$ production determines the electrons available for mediated electron transfer in MES, the differences between the GAC electrodes were determined. The control GAC did not produce $H_2$, and the current density remained low, at ca. 0.3 ± 0.01 mA $cm^{-3}$. Cu-GAC, on the other hand, resulted in $H_2$ evolution of 2.6 ± 0.2 $m^3\ m^{-3}\ d^{-1}$ with average current density of 3.7 ± 0.3 mA $cm^{-3}$. The highest $H_2$ evolution of 4.5 ± 0.4 $m^3\ m^{-3}\ d^{-1}$ and average current density of 6.5 ± 0.3 mA $cm^{-3}$ were obtained with Ni-GAC. These experiments indicated the superior performance of Ni and Cu impregnated GAC for $H_2$ evolution, which is hypothesized to be beneficial for $H_2$ mediated VFA production in MES.

### 3.2. Microbial electrosynthesis with metal impregnated granules

#### 3.2.1. Carboxylate production

VFA production in MES started during the first one to four days of the runs. Similarly to the abiotic experiments, considerably higher performance, *i.e.* higher VFA production rates, was observed in MES with Ni and Cu impregnated GAC than without metal impregnation (Fig. 3). Acetate was the main VFA produced, while butyrate was produced with Ni-GAC and Cu-GAC in the second run from day 25 onwards with overall titers of 4.1 and 2.7 g/L, respectively. The acetate production was similar with the metal impregnated GAC with slightly higher acetate titers and production rates with Cu-GAC (6.4–7.0 g/L and 222–241 mg/L $d^{-1}$, respectively) than with Ni-GAC (5.2–6.3 g/L and 180–216 mg/L $d^{-1}$, respectively). This is in contradiction with the abiotic experiments, where 1.8-fold higher current density was obtained with Ni-GAC compared to Cu-GAC. Without metal impregnation, acetate was produced only in one of the parallel reactors (Fig. 3) resulting in acetate titers and acetate production rates from 0 to 2.0 g/L and from 0 to 111 mg/L $d^{-1}$, respectively. The cathodic efficiencies for acetate production varied on average between 0–26 % for GAC without metal impregnation, 21–37 % for Cu-GAC, and 13–28 % for Ni-GAC. Although $H_2$ production was not measured during the MES runs, $H_2$ evolution likely accounted for high portion of the cathodic efficiencies as reported earlier (*e.g.*, Yao et al., 2024).

The acetate titers and production rates of this study are in similar

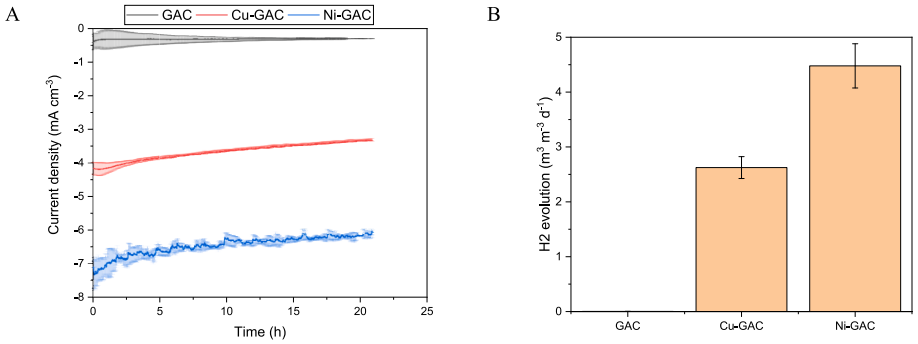


**Fig. 2.** Current densities and $H_2$ evolution obtained in abiotic electrochemical runs with Ni- (Ni-GAC) and Cu-impregnated GAC (Cu-GAC) as well as with GAC without metal impregnation (GAC). The error bars show the standard deviation of the three consecutive runs.

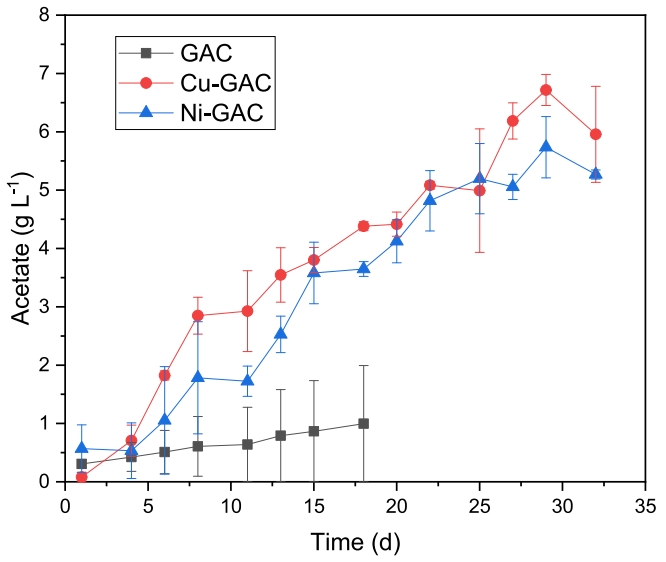


**Fig. 3.** Acetate concentrations obtained in MES with Ni- (Ni-GAC) and Cu-impregnated GAC (Cu-GAC) as well as without metal impregnation (GAC) in two parallel runs (GAC-1 and GAC-2). The results are mean values from two parallel MES runs with standard deviations.

range or higher than what has been reported earlier with metal impregnated GAC when compared via normalizing the results against the GAC volume and/or mass, which is considered important as the GAC is used as the electrode materials and serves as the surface area for the growth of biofilm and for electrocatalytic activities. In this study, the acetate production rates and current densities normalized against the volume of the GAC at the cathode were 3.1–3.7 and 4.0–4.1 mg $m^{-3}$ $d^{-1}$ for the Ni-GAC and Cu-GAC, respectively, resulting in current densities from 2.0 to 5.6 mA $cm^{-3}$ and from 1.9 to 3.4 mA $cm^{-3}$ (*i.e.*, from 4.3 to 12.1 mA $g^{-3}$ and from 4.0 to 7.3 mA $g^{-3}$, normalized against the mass of GAC cathode). For example, MES with Ni impregnated GAC with high Ni loading (5 wt%) resulted in acetate titers of over 3 g/L with current density between 1 and 3 mA $cm^{-3}$ (between 6.4 and 19 mA $g^{-3}$) (Chatzipanagiotou et al., 2022). GAC impregnated with $Fe_3O_4$ (38 wt%) resulted in acetate titers and production rates of 5.1 g/L and 171 mg/L $d^{-1}$, respectively, with current density of 2.8 mA $g^{-3}$ (Zhu et al., 2019). A similar acetate production rate of 204 ± 2 mg/L $d^{-1}$ (1.8 mg $m^{-3}$ $d^{-1}$) was obtained with packed GAC bed without metal impregnation in our previous study (Vassilev et al., 2024), in which the amount of GAC used was double compared to the current study resulting in current densities of 0.8 ± 0.3 mA $cm^{-3}$ (1.8 ± 0.7 mA $g^{-3}$). Overall, the normalized acetate production rates and current densities are among the highest reported in the selected studies. Metal catalysts have been reported to enhance $H_2$ evolution and subsequently acetate and/or methane production in MES (Jourdin et al., 2016; Kracke et al., 2019), which is the likely reason for improved VFA production also in this study. This hypothesis is supported by the abiotic $H_2$ production experiments that showed improved current densities and $H_2$ evolution when utilizing copper and nickel impregnated granules.

In this study, the current densities differed between the consecutive runs. With control reactors, the average current densities were 0.23 ± 0.05 mA $cm^{-3}$ and 1.1 ± 0.9 mA $cm^{-3}$ in the first and second runs, respectively (see supplementary material), resulting in slightly lower pH values (between 6.8 and 7.0 *vs.* 6.6–6.3) and higher acetate production (2.0 *vs.* 0.0 g/L) in the second run with the higher current density. With Cu-GAC considerably higher average current densities were obtained in the first run compared to the second run, *i.e.,* 3.4 ± 0.5 mA $cm^{-3}$ and 1.9 ± 1.1 mA $cm^{-3}$, respectively, while with Ni-GAC the opposite trend was observed with higher average current densities obtained with the second run compared to the first run, *i.e.,* 5.6 ± 0.7 mA $cm^{-3}$ and 2.0 ± 1.0 mA $cm^{-3}$, respectively. With Cu and Ni impregnated GAC, however, the varying average current densities between the two runs did not affect the acetate titers or production rates considerably indicating that current density was not limiting acetate production. Additional studies were conducted to understand how the packing of the GAC bed (with GAC without metal impregnation) affects their electrochemical performance. Increasing the supplied force from 0.2 to 1.6 Nm decreased the contact resistance from 0.27 ± 0.12 Ω to 0.13 ± 0.01 Ω (see Supplementary material). This shows that pressing the GAC bed at different forces has an effect on contact resistance and hence, also the current densities. This is one likely reason for the different current densities observed during the two consecutive MES runs and highlights the importance of controlling the force used to pack the GAC beds, when packed beds are used for MES. Although the force used to pack the GAC bed likely affected the current densities, the current densities and acetate yields obtained with the metal impregnated GAC were considerably higher than with the bare GAC, highlighting the advantages of using metal catalysts on GAC.

With Cu-GAC and Ni-GAC, the pH decreased in time from ca. 7.0 to 6.0 (see supplementary material). In similar MES studies where $CO_2$ was fed three to five times a week for 10–15 min, availability of $CO_2$ hindered carboxylate production in MES (Vassilev et al., 2024; Yao et al., 2024), which is the likely reason in the current study and would explain the similar carboxylate production observed with Ni-GAC and Cu-GAC despite of the varying current densities. However, as total inorganic carbon was not measured in the current study, this cannot be verified.

The other potential reasons for the differences in the current densities between the two consecutive runs were further studied. Due to the large decrease in the current density of Cu-GAC both during the MES runs and in the CVs measured before the MES runs (see Chapter 3.2.2), it was hypothesized that the storage of the metal impregnated granules or the abiotic electrochemical characterizations done before the biological experiments could affect the characteristics of the granules. Increase in current density, especially observed during the two consecutive biological MES runs with the GAC without metal impregnation as well as with Ni-GAC, could be due to metal leaching observed during the MES runs and/or due to the packing of the bed that was done manually (as the forces used for packing the bed were not measured when constructing the MES runs). Thus, the characteristics of the metal impregnated GAC were analyzed in detail and the results are reported in the following chapter.

### *3.2.2. Effects of storage and microbial electrosynthesis runs on metal impregnated granules*

The large changes in the current densities of Ni and Cu impregnated GAC in the parallel MES runs (see supplementary material) indicated that the GAC had different electrochemical behavior between the two consecutive runs. A similar phenomenon was also observed in abiotic CVs that were run before the MES runs (Fig. 4). With control GAC, the maximum current densities at −0.85 V were 0.6 and 2.1 mA $cm^{-3}$ in the CVs performed before the first and second MES runs, respectively, and differences in the capacitance were observed. With Cu-GAC and Ni-GAC lower current densities in CVs were observed before the second MES run, after storing the GAC under air for ca. four months. With Cu-GAC, the maximum current density obtained in CVs before the first MES run was 4.3 mA $cm^{-3}$, which was decreased to 2.3 mA $cm^{-3}$ before the second MES run. Similarly with Ni-GAC, the maximum current density was decreased from 5.6 to 3.7 mA $cm^{-3}$ between the first and second MES runs, respectively. To determine whether some changes in the GAC characteristics occurred during the storage, the Cu and Ni content as well as their oxidation stages were determined from freshly prepared metal impregnated granules and after ca. eight months of storage under air atmosphere as well as from the metal impregnated granules after the MES runs (Tables 2 and 3).

From the initial Cu and Ni contents in the GAC of 47 and 45 mg $g^{-1}_{granule}$, respectively, the metal contents decreased during the abiotic CV

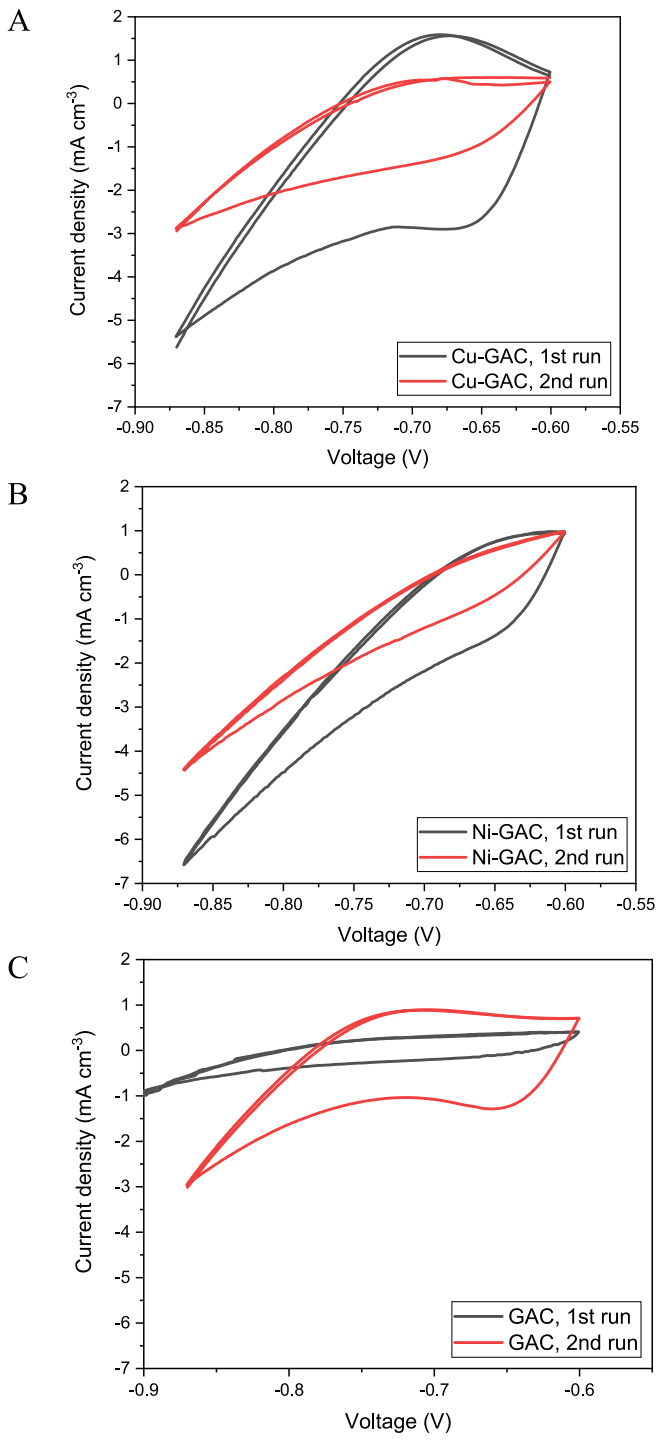


**Fig. 4.** Cyclic voltammetry (CV) measurements with granules impregnated with A) Cu (Cu-GAC) or B) Ni (Ni-GAC), and C) without metal impregnation (GAC). CVs were run before the first and second biological MES runs (1st run and 2nd run, respectively). The current densities are given against the volume of the GAC.

and MES runs (Table 2). With Cu-GAC, the Cu content was higher after the first MES run compared to the second MES run, being 31.8 and 17.6 mg $g^{-1}_{granule}$, respectively. This correlates with the current densities, as both the current densities in the CVs before MES runs and current densities during MES runs were higher in the first compared to the second run. With Ni-GAC the Ni content was higher after the second MES run, 40.4 mg $g^{-1}_{granule}$ compared to 29.8 mg $g^{-1}_{granule}$ after the first MES run, which again correlates with the higher current densities obtained during

**Table 2**
The Cu and Ni content of granular activated carbon (GAC) after the first and second microbial electrosynthesis runs with granules impregnated with Cu (Cu-GAC) or Ni (Ni-GAC) or without metal impregnation (GAC). Note that different GAC batches were used for the two different MES runs.

| Sample | Cu (mg $g^{-1}_{granule}$) | Ni (mg $g^{-1}_{granule}$) |
|---|---|---|
| GAC – Fresh | 0.13 | 0.05 |
| GAC – After MES | 0.13 ± 0.01 | 0.07 ± 0.02 |
| Cu-GAC – Fresh | 47 | 0.08 |
| Cu-GAC – After MES | 25 ± 10 | 0.11 ± 0.05 |
| Ni-GAC – Fresh | 0.17 | 4 |
| Ni-GAC – After MES | 0.13 ± 0.00 | 35 ± 8 |

**Table 3**
Binding energies [eV] of Cu $2p_{3/2}$ or Cu and Ni $2p_{3/2}$ or Ni species, and their relative contents (in parentheses) of freshly prepared granular activated carbon impregnated with copper (Cu-GAC), after storage of 8 months under air atmosphere and after the first and second microbial electrosynthesis (MES) runs.

| Sample | $Cu_2O$ | CuO |
|---|---|---|
| Cu-GAC fresh | 932.78 (0.56) | 934.35 (0.44) |
| Cu-GAC after 8 months of storage under air | 933.02 (0.54) | 934.75 (0.46) |
| Cu-GAC after first MES run | 933.13 (0.44) | 935.64 (0.56) |
| Cu-GAC after second MES run | 932.82 (0.44) | 933.84 (0.56) |
| | **NiO** | **$Ni(OH)_2$** |
| Ni-GAC fresh | 854.56 (0.10) | 856.23 (0.90) |
| Ni-GAC after 8 months of storage under air | 854.75 (0.18) | 856.07 (0.82) |
| Ni-GAC after first MES run | n.d. | 856.67 (1.00) |
| Ni-GAC after second MES run | n.d. | 856.50 (1.00) |

n.d. = not detected.

the second MES run indicating that leaching of nickel in the first MES run likely negatively affected the current densities. However, lower current densities were obtained in the CVs before the second MES run compared to the first run, which indicates that nickel leaching likely occurred either during the MES run or during the $H_2$ production tests performed between the first CVs and MES runs. However, as the metal content on the granules were not characterized after the CVs and $H_2$ evolution tests, this could not have been experimentally proven and should be further studied. As expected, only trace amounts of Cu or Ni were observed in GAC without metal impregnation. The results indicate that higher metal content in GAC results in higher current densities in MES runs but does not clarify at which stage of the experiments the metals are leached from the GAC.

Leaching of metals from cathode electrodes has been observed before, for example, in MES where activated carbon was impregnated with 5 % wt Ni resulting in up to 5 % leaching of Ni (Chatzipanagiotou et al., 2022) and when using metal mix-based catalyst resulting in decreased current densities upon leaching of certain metal elements, including Mn, Mo, Ni and Zn when ethylenediaminetetraacetic acid (EDTA) was used when preparing the catalyst (de Smit et al., 2024). Also in this study, metal leaching decreased the current densities, although acetate production in MES was not affected due to current not likely being the limiting factor. Furthermore, it has been reported that nickel loading of 0.01 % wt already improved acetate production by 3-fold (Chatzipanagiotou et al., 2022). Thus, as the copper and nickel content in this study decreased down to 1.8 wt% and 3.0 wt%, respectively, this content did not negatively affect VFA production yet. However, to ensure a long-term performance of MES, also in conditions where current density becomes limiting factor, methodologies for inserting metal catalysts on carbon support should be further studied to enable better stability of the metal catalysts in the MES conditions. In this study, the metals were impregnated on the surface of the GAC via dry impregnation followed by calcination, while, for example, hydrothermal process (Bian et al., 2024) or electrodeposition (Gomez Vidales et al., 2021) have been used to prepare metallic catalysts for MES with NiMo or Ni

and Fe, respectively. Furthermore, the optimal loading of metal catalyst on the GAC should be delineated.

The XPS analysis was carried out to study the oxidation states of the Cu and Ni on the surfaces of GACs. Both fresh GAC, GAC after 8 months of storage, and samples after abiotic CV and MES runs were analyzed. The $Ni_2p$ and $Cu_2p$ spectra and their Gaussian-Lorentz mixed fitting figures are shown in supplementary material (see supplementary material) and the binding energies (BEs) and relative contents of Ni and Cu species in Table 3. In Cu-GACs, Cu spectra can be fitted into two peaks, namely $Cu_2O$ and CuO. The BEs in the range of 932.1–933.1 eV can be attributed to the $Cu^+$ (Biesinger et al., 2010; Yang et al., 2019) and the BEs at 933.8–935.6 eV to $Cu^{2+}$ (Chen et al., 2022; Zhang et al., 2015). However, it should be noted that the BEs of $Cu^0$ and $Cu^+$ are close to each other's (Zhang et al., 2015), so metallic copper can also be present, especially in the fresh material (see supplementary material). During storage time (8 months) the relative amount of $Cu^{2+}$ was slightly increased compared to $Cu^+$ but the difference was more obvious in Cu-GACs after MES runs in which CuO was the main species. Thus, storage of Cu-GAC had only a slight effect on the oxidation stage of Cu, while during MES runs Cu was further oxidized towards CuO. Therefore, oxidation of Cu during storage of Cu-GAC granules under air atmosphere cannot explain the decreased performance of Cu impregnated granules in abiotic CV and biological MES runs.

As with the Cu-GACs, Ni-GACs spectra can be deconvoluted into two peaks (see supplementary material) in fresh materials (Table 3). The BEs in the range of 854.6–854.8 eV can be assigned to NiO (Czekaj et al., 2007; Gonçalves et al., 2020), while the BEs in the range 856.1–856.7 eV can be attributed to the $Ni(OH)_2$ (Czekaj et al., 2007; Mahata et al., 2008). No elemental Ni was observed in any of the Ni-GACs. The relative amount of NiO was low already in fresh Ni-GACs (both fresh and after 8 months storage), and in Ni-GACs after MES runs Ni had been oxidized to $Ni^{2+}$ ($Ni(OH)_2$) and no $Ni^+$ (NiO) was observed. As with Cu-GAC, with Ni-GAC also the changes in the oxidation state of Ni were so small that they were likely not the reason for the decreased current densities during the abiotic CVs. Thus, the content of Cu and Ni (Table 2) have a more important role in the obtained current densities.

## 4. Conclusions

Nickel and copper impregnated GAC resulted in improved abiotic current densities, from 0.3 up to 6.5 mA $cm^{-3}$, compared to GAC without metals. Similarly, considerably higher current densities and acetate production rates, from 0.2 up to 5.6 mA $cm^{-3}$ and from zero up to 241 mg $L^{-1}$ $d^{-1}$, respectively, were obtained in MES with metal impregnated granules. The metal content on granules decreased during the runs and affected the current densities, although did not limit acetate production in MES, while the oxidation state of the metal did not considerably affect the current densities and MES performance.

## CRediT authorship contribution statement

**Igor Vassilev:** Writing – review & editing, Methodology, Conceptualization. **Hui Yao:** Writing – review & editing, Investigation. **Sadaf Shakeel:** Writing – original draft. **Markus Tuominen:** Investigation. **Anne Heponiemi:** Writing – original draft, Investigation, Formal analysis, Conceptualization. **Davide Bergna:** Writing – original draft, Resources, Investigation, Conceptualization. **Ulla Lassi:** Writing – review & editing, Supervision, Funding acquisition, Conceptualization. **Marika Kokko:** Writing – original draft, Visualization, Supervision, Funding acquisition.

## Declaration of competing interest

The authors declare the following financial interests/personal relationships which may be considered as potential competing interests: Marika Kokko reports financial support was provided by Research Council of Finland. Ulla Lassi reports financial support was provided by Research Council of Finland. If there are other authors, they declare that they have no known competing financial interests or personal relationships that could have appeared to influence the work reported in this paper.

## Acknowledgements

The authors acknowledge the funding from Research Council of Finland (grant numbers 316657, 319910, 346046, 329227 and 329228). Furthermore, the Research Council of Finland (Bio and Circular Economy Research Infrastructure (decision No. 353658)) is gratefully acknowledged. The authors would like to thank Mika Karttunen for helping with MES reactor configuration at Tampere University. Special thanks to Markus Väyrynen, Juhani Väisänen, Sari Tuikkanen, Riikka Koski, Hanna Prokkola and Venla Rantala for their assistance in the experimentation. The authors thank the staff of the Center of Microscopy and Nanotechnology, University of Oulu, for their assistance during the XPS analyses, and acknowledge Prof. Annemiek ter Heijne, Wageningen University & Research, for providing laboratory facilities for testing the effects of packing of GAC bed on current densities.

## Appendix A. Supplementary data

Supplementary data to this article can be found online at https://doi.org/10.1016/j.biortech.2024.131914.

## Data availability

Data will be made available on request.

## References

Bian, B., Yu, N., Akbari, A., Shi, L., Zhou, X., Xie, C., Saikaly, P.E., Logan, B.E., 2024. Using a non-precious metal catalyst for long-term enhancement of methane production in a zero-gap microbial electrosynthesis cell. Water Res. 259, 121815. https://doi.org/10.1016/j.watres.2024.121815.

Biesinger, M.C., Lau, L.W.M., Gerson, A.R., Smart, R., St, C., 2010. Resolving surface chemical states in XPS analysis of first row transition metals, oxides and hydroxides: Sc, Ti, V, Cu and Zn. Appl. Surf. Sci. 257, 887–898. https://doi.org/10.1016/j.apsusc.2010.07.086.

Brunauer, S., Emmett, P.H., Teller, E., 1938. Adsorption of gases in multimolecular layers. J. Am. Chem. Soc. 60, 309–319. https://doi.org/10.1021/ja01269a023.

Caizán-juanarena, L., Servin-balderas, I., Chen, X., Buisman, C.J.N., 2019. Electrochemical and microbiological characterization of single carbon granules in a multi-anode microbial fuel cell. J. Power Sources 435, 126514. https://doi.org/10.1016/j.jpowsour.2019.04.042.

Chatzipanagiotou, K.-R., Jourdin, L., Bitter, J.H., Strik, D.P.B.T.B., 2022. Concentration-dependent effects of nickel doping on activated carbon biocathodes. Catal. Sci. Technol. 12, 2500–2518. https://doi.org/10.1039/D1CY02151F.

Chen, X., Feng, X., Xie, Y., Wang, L., Chen, L., Wang, X., Ma, Y., Ning, P., Pu, Y., 2022. Investigation of the role of copper species-modified active carbon by low-temperature roasting on the improvement of arsine adsorption. ACS Omega 7, 17358–17368. https://doi.org/10.1021/acsomega.2c01355.

Czekaj, I., Loviat, F., Raimondi, F., Wambach, J., Biollaz, S., Wokaun, A., 2007. Characterization of surface processes at the Ni-based catalyst during the methanation of biomass-derived synthesis gas: X-ray photoelectron spectroscopy (XPS). Appl. Cat. A: General 329, 68–78. https://doi.org/10.1016/j.apcata.2007.06.027.

Dadkhah, M., Tulliani, J.-M., 2022. Nanostructured metal oxide semiconductors towards greenhouse gas detection. Chemosensors 10, 57. https://doi.org/10.3390/chemosensors10020057.

de Smit, S.M., van Mameren, T.D., van Zwet, K., van Veelen, H.P.J., Cristina Gagliano, M., Strik, D.P.B.T.B., Bitter, J.H., 2024. Integration of biocompatible hydrogen evolution catalyst developed from metal-mix solutions with microbial electrosynthesis. Bioelectrochem. 158, 108724. https://doi.org/10.1016/j.bioelechem.2024.108724.

Gibert, O., Lefèvre, B., Fernández, M., Bernat, X., Paraira, M., Calderer, M., Martínez-Lladó, X., 2013. Characterising biofilm development on granular activated carbon used for drinking water production. Water Res. 47, 1101–1110. https://doi.org/10.1016/j.watres.2012.11.026.

Gomez Vidales, A., Bruant, G., Omanovic, S., Tartakovsky, B., 2021. Carbon dioxide conversion to C1–C2 compounds in a microbial electrosynthesis cell with in situ electrodeposition of nickel and iron. Electrochim. Acta 383, 138349. https://doi.org/10.1016/j.electacta.2021.138349.

Gonçalves, L.P.L., Sousa, J.P.S., Soares, O.S.G.P., Bondarchuk, O., Lebedev, O.I., 2020. The role of surface properties in CO2 methanation over carbon-supported Ni catalysts and their promotion by Fe. Catal. Sci. Technol. 10, 7217–7225. https://doi.org/10.1039/D0CY01254H.

Gong, M., Zhou, W., Tsai, M.-C., Zhou, J., Guan, M., Lin, M.-C., Zhang, B., Hu, Y., Wang, D.-Y., Yang, J., Pennycook, S.J., Hwang, B.-J., Dai, H., 2014. Nanoscale nickel oxide/nickel heterostructures for active hydrogen evolution electrocatalysis. Nat. Commun. 5, 4695. https://doi.org/10.1038/ncomms5695.

Huang, Q., Wang, X., Li, J., Dai, C., Gamboa, S., Sebastian, P.J., 2007. Nickel hydroxide/activated carbon composite electrodes for electrochemical capacitors. J. Power Sources 164, 425–429. https://doi.org/10.1016/j.jpowsour.2006.09.066.

Jourdin, L., Lu, Y., Flexer, V., Keller, J., Freguia, S., 2016. Biologically induced hydrogen production drives high rate/high efficiency microbial electrosynthesis of acetate from carbon dioxide. ChemElectroChem 3, 581–591. https://doi.org/10.1002/celc.201500530.

Kim, K.-R., Kang, J., Chae, K.-J., 2017. Improvement in methanogenesis by incorporating transition metal nanoparticles and granular activated carbon composites in microbial electrolysis cells. Int. J. Hydrogen Energy 42, 27623–27629. https://doi.org/10.1016/j.ijhydene.2017.06.142.

Kracke, F., Wong, A.B., Maegaard, K., Deutzmann, J.S., Hubert, M.A., Hahn, C., Jaramillo, T.F., Spormann, A.M., 2019. Robust and biocompatible catalysts for efficient hydrogen-driven microbial electrosynthesis. Commun. Chem. 2, 45. https://doi.org/10.1038/s42004-019-0145-0.

Lastoskie, C., Gubbins, K.E., Quirke, N., 1993. Pore size heterogeneity and the carbon slit pore: a density functional theory model. Langmuir 9, 2693–2702. https://doi.org/10.1021/la00034a032.

Li, J.-L., Takeguchi, T., Inui, T., 1996. Doping effect of potassium permanganate on the performance of a copper/zinc oxide/alumina catalyst for methanol formation. Appl. Cat. A: General 139, 97–106. https://doi.org/10.1016/0926-860X(96)00022-1.

Mahata, N., Cunha, A.F., Órfão, J.J.M., Figueiredo, J.L., 2008. Hydrogenation of nitrobenzene over nickel nanoparticles stabilized by filamentous carbon. Appl. Cat. A: General 351, 204–209. https://doi.org/10.1016/j.apcata.2008.09.015.

Moreno-Jimenez, D.A., Kumaran, Y., Efstathiadis, H., Hwang, M.-H., Jeon, B.-H., Kim, K.-Y., 2023. Flowable nickel-loaded activated carbon cathodes for hydrogen production in microbial electrolysis cells. ACS EST Eng. 3 (10), 1476–1485. https://doi.org/10.1021/acsestengg.3c00122.

Newsome, D.S., 1980. The water-gas shift reaction. Cat. Rev. 21, 275–318. https://doi.org/10.1080/03602458008067535.

Nie, H., Zhang, T., Cui, M., Lu, H., Lovley, D.R., Russell, T.P., 2013. Improved cathode for high efficient microbial-catalyzed reduction in microbial electrosynthesis cells. Phys. Chem. Chem. Phys. 15, 14290–14294. https://doi.org/10.1039/C3CP52697F.

Park, S.-G., Rhee, C., Shin, S.G., Shin, J., Mohamed, H.O., Choi, Y.-J., Chae, K.-J., 2019. Methanogenesis stimulation and inhibition for the production of different target electrobiofuels in microbial electrolysis cells through an on-demand control strategy using the coenzyme M and 2-bromoethanesulfonate. Environ. Int. 131, 105006. https://doi.org/10.1016/j.envint.2019.105006.

Vassilev, I., Hernandez, P.A., Batlle-Vilanova, P., Freguia, S., Krömer, J.O., Keller, J., Ledezma, P., Virdis, B., 2018. Microbial electrosynthesis of isobutyric, butyric, caproic acids, and corresponding alcohols from carbon dioxide. ACS Sust. Chem. Eng. 6, 8485–8493. https://doi.org/10.1021/acssuschemeng.8b00739.

Vassilev, I., Rinta-Kanto, J.M., Kokko, M., 2024. Comparing the performance of fluidized and fixed granular activated carbon beds as cathodes for microbial electrosynthesis of carboxylates from CO2. Biores. Technol. 403, 130896. https://doi.org/10.1016/j.biortech.2024.130896.

Vij, V., Sultan, S., Harzandi, A.M., Meena, A., Tiwari, J.N., Lee, W.-G., Yoon, T., Kim, K. S., 2017. Nickel-based electrocatalysts for energy-related applications: oxygen reduction, oxygen evolution, and hydrogen evolution reactions. ACS Catal. 7, 7196–7225. https://doi.org/10.1021/acscatal.7b01800.

Wang, L., He, Z., Guo, Z., Sangeetha, T., Yang, C., Gao, L., Wang, A., Liu, W., 2019. Microbial community development on different cathode metals in a bioelectrolysis enhanced methane production system. J. Power Sources 444, 227306. https://doi.org/10.1016/j.jpowsour.2019.227306.

Yang, S., Wang, D., Liu, H., Liu, C., Xie, X., Xu, Z., Liu, Z., 2019. Highly stable activated carbon composite material to selectively capture gas-phase elemental mercury from smelting flue gas: Copper polysulfide modification. Chem. Eng. J. 358, 1235–1242. https://doi.org/10.1016/j.cej.2018.10.134.

Yao, H., Rinta-Kanto, J.M., Vassilev, I., Kokko, M., 2024. Methanol as a co-substrate with CO2 enhances butyrate production in microbial electrosynthesis. Appl. Microbiol. Biotechnol. 108, 372. https://doi.org/10.1007/s00253-024-13218-y.

Zhang, S., Jiang, J., Wang, H., Li, F., Hua, T., Wang, W., 2021. A review of microbial electrosynthesis applied to carbon dioxide capture and conversion: the basic principles, electrode materials, and bioproducts. J. CO2 Utiliz. 51, 101640. https://doi.org/10.1016/j.jcou.2021.101640.

Zhang, G., Li, Z., Zheng, H., Fu, T., Ju, Y., Wang, Y., 2015. Influence of the surface oxygenated groups of activated carbon on preparation of a nano Cu/AC catalyst and heterogeneous catalysis in the oxidative carbonylation of methanol. Appl. Cat. B: Environ. 179, 95–105. https://doi.org/10.1016/j.apcatb.2015.05.001.

Zhang, T., Nie, H., Bain, T.S., Lu, H., Cui, M., Snoeyenbos-West, O.L., Franks, A.E., Nevin, K.P., Russell, T.P., Lovley, D.R., 2013. Improved cathode materials for microbial electrosynthesis. Energy Environ. Sci. 6, 217–224. https://doi.org/10.1039/C2EE23350A.

Zhu, H., Dong, Z., Huang, Q., Song, T., Xie, J., 2019. Fe3O4/granular activated carbon as an efficient three-dimensional electrode to enhance the microbial electrosynthesis of acetate from CO2. RSC Adv. 9, 34095–34101. https://doi.org/10.1039/C9RA06255F.